What added value of CNRM-AROME convection-permitting regional climate model compared to CNRM-ALADIN regional climate model for urban climate studies? Evaluation over Paris area (France)

A. Lemonsu, C. Caillaud, A. Alias, S. Riette, Y. Seity, B. Le Roy, Y. Michau, P. Lucas-Picher

What added value of CNRM-AROME convection-permitting regional climate model compared to CNRM-ALADIN regional climate model for urban climate studies ? Evaluation over Paris area (France)

Lemonsu A.[1], Caillaud C.[1], Alias A.[1], Riette S.[1], Seity Y.[1], Le Roy B.[2,3], Michau Y.[1], Lucas-Picher P. [4]

[1] CNRM, Université de Toulouse, Météo-France, CNRS, Toulouse, France
[2] Princeton University, Cooperative Institute for Modeling the Earth System, Princeton, NJ 08540, USA
[3] NOAA, Geophysical Fluid Dynamics Laboratory, Princeton, NJ 08540, USA
[4] Département des sciences de la Terre et de l'atmosphère, Université du Québec à Montréal, Montréal, Canada

Corresponding author: Aude Lemonsu, aude.lemonsu @meteo.fr

ORCID

Aude Lemonsu	http://orcid.org/0000-0001-8894-0088
Cécile Caillaud	http://orcid.org/0000-0003-2317-4129
Antoinette Alias	http://orcid.org/0000-0002-8886-2830
Sébastien Riette	http://orcid.org/0000-0002-0142-4580
Yann Seity	
Benjamin Le Roy	http://orcid.org/0000-0002-5496-2462
Yohanna Michau	http://orcid.org/0000-0003-0781-9783
Philippe Lucas-Picher	http://orcid.org/0000-0001-8707-7745

Abstract

The convection-permitting regional climate model CNRM-AROME was applied on a spatial domain restricted to the northern half of France for analyzing its performances in simulating the urban climate of Paris region, and its potential added value compared to the regional climate model CNRM-ALADIN. In addition to its fine horizontal resolution (2.5 km compared to 12.5 km for CNRM-ALADIN), CNRM-AROME has the advantage of integrating the urban canopy model TEB into its land-surface modelling system. A hindcast simulation was performed for the past period 2000-2017, following an evaluation configuration for which CNRM-AROME was driven by CNRM-ALADIN, driven itself by the ERA-Interim reanalyses. Long-term gridded observations with kilometric resolution allowed a fine spatial scale evaluation of the atmospheric variables simulated by both models. They showed in particular a significant overestimation of spring precipitation, but an improvement of summer precipitation in CNRM-AROME compared to CNRM-ALADIN. Above all, thanks to its horizontal resolution and the use of a dedicated urban model, CNRM-AROME was shown to offer significant added value for the simulation of urban heat islands, for the mapping of heat-warming areas, and for representing the effects of the city on precipitation. It is a promising tool to diagnose climatic and impact indicators at the city scale, and their evolution in a changing climate.

Keywords Convection-permitting regional climate model · Urban canopy model · Paris urban area · Urban heat island · Heat warming · Precipitation

1. Introduction

Urban covers are a modification of the natural environment, mainly through the artificialization and sealing of soils and the implementation of built-up infrastructures with complex three-dimensional morphology. This results in a significant modification of the radiation, energy, momentum, and water exchanges at the interface between surface and atmosphere (Oke et al. 2017). These physical processes related to the urban environment generate locally specific microclimatic conditions referred to as the urban climate. This is particularly the case within the urban canopy layer, which designates the area extending from the ground to the tops of buildings, and which includes all the elements that make up the urban landscape and the volume of ambient air. The urban heat island (UHI) phenomenon can be observed at this level. It results in higher

near-surface air temperatures in the city than in the surrounding natural areas during the night. Its intensity depends on the characteristics of the city itself (i.e. materials properties, morphology and compactness, anthropogenic heat emissions, Tong et al. 2017; Zhang et al. 2021), the land use land cover around the city, and the regional environment (Bokwa et al. 2015; Santamouris et al. 2017; Kassomenos et al. 2022). It is also strongly governed by weather conditions of the day, e.g. sunlight, cloud cover, wind, temperature, etc. (He 2018; Nagarambe et al. 2021), which makes it a variable phenomenon on both daily and seasonal scales. But the effects of urban areas extend beyond the urban canopy layer. They can also impact the atmospheric boundary layer, its characteristics of temperature, humidity, wind, turbulence, its vertical structure, and its dynamics with time (Melecio-Vázquez 2018; Wang et al. 2021). As a result, cities can interact with local or even regional weather and climate, and change environmental conditions. In particular, studies have shown effects on atmospheric circulation, cloud cover, and precipitation (Lorentz et al. 2019; Theeuwes et al. 2019; Tsiringakis et al. 2022).

In addition to the urban climate, cities are facing global changes already underway that combine climate change and urban expansion associated with demographic pressure. The environmental issues and risks we already experience in cities could be exacerbated by these global changes (IPCC 2022). In particular, there is evidence that heat-wave conditions, which are expected to become much more frequent and severe in the future, are conducive to very strong UHI (Tan et al. 2010; Founda and Santamouris 2017; Yang et al. 2019). That already leads to important issues of energy consumption for air conditioning, thermal discomfort, and even morbidity and mortality (Laaidi et al. 2012; Schinasi et al. 2018), which could become even more of a concern. This observation motivates the implementation of impact studies in cities, that means impacts of urban climate, climate change, or combined effects, in order to prepare adaptation.

This type of study raises some methodological questions. The climate projections from the climate model intercomparison project (CMIP) are provided by global circulation models (GCMs) with too loose horizontal resolution. The use of limited area regional climate models (RCMs) allows an interesting dynamical downscaling to better deal with surface heterogeneities and local phenomena, thanks to better spatial resolution and specific physical and dynamic parameterizations. For example, a set of climate projections at 0.11° (~12.5 km) resolution is available for Europe on the basis of the Euro-CORDEX research initiative (Jacob et al. 2014). Nevertheless, the dozen kilometers of resolution - sufficient for some impact studies - remains a strong limitation for the city scale and the description of urban land uses. On the other hand, most of the surface parameterizations applied in these RCMs do not address the specificities of urban areas and the physical processes associated with them (Masson et al. 2020). On the basis of simulations with the RCM ALADIN applied on Metropolitan France at 0.11° resolution and coupled with the urban model TEB, Daniel et al. (2019) have demonstrated the relevance and benefits of activating a dedicated urban canopy model in climate simulations. They showed the significant impact of cities on near-surface temperatures, beyond the geographical limits of urban areas, which highlights the feedback of urban climate on regional climate. They also found that the TEB model was able to simulate more realistic nighttime UHI than the standard approach applied by most RCMs that describe cities as rocky surfaces.

A new generation of very high resolution RCMs has recently been developed. Initially motivated by the need to better represent convective phenomena, these models called convection-permitting regional climate models (CP-RCM) have resolutions of 1 to 3 km, are non-hydrostatic, and explicitly resolve deep convection (Prein et al. 2015; Lucas-Picher et al. 2021). They provide a particularly interesting climate modeling framework for urban studies. In particular, the French weather prediction model CNRM-AROME has been used since 2014 in climate-simulation configuration with a horizontal resolution of 2.5 km. It has been applied on a pan-Alpine domain for the CORDEX convection flagship pilot study (Coppola et al. 2020) with a focus on the study of extreme precipitation over the Mediterranean area (Fumière et al. 2020; Caillaud et al. 2021), and more recently on an extended France domain for the European project EUCP (EUropean Climate Prediction system, Hewitt et al. 2018). CNRM-AROME was here applied on a spatial domain restricted to the northern half of France for a specific analysis of its performances in simulating the urban

climate of the Paris region, and of the potential added value compared to the RCM CNRM-ALADIN. With this aim, a simulation was performed for the past period 2000-2017 following an evaluation configuration for which CNRM-AROME is driven by CNRM-ALADIN which is driven itself by the ERA-Interim reanalyses. The choice of the Paris region is motivated first by the urban context, since the Paris metropolitan area is the largest and most populated in France, and second, by the availability of observational data allowing possible a climatological-scale evaluation of the simulation and of some urban effects.

2. Description of models and configurations

2.1 Evaluation run configuration

The climate modeling framework follows an "evaluation run" configuration for which large-scale conditions were provided by the ERA-Interim reanalyses (Dee et al. 2011) released from the European Center for Medium-Range Weather Forecasts over the globe with a 80 km horizontal resolution. These reanalyses drove a dynamic spatial downscaling based on two successive limited-area RCMs with respective horizontal resolutions of 12.5 km and 2.5 km (see domains in Figure 1). The intermediate RCM was CNRM-ALADIN (Aire Limitée Adaptation dynamique Développement InterNational, in French) in its most recent version v6.3 (Daniel et al. 2019; Nabat et al. 2020) applied to a Euro-CORDEX domain of about 5900 km × 5900 km. CNRM-ALADIN drove the CP-RCM CNRM-AROME that ran over the whole northern part of France for a domain of 640 km × 640 km. The domain was chosen large enough to ensure the CP-RCM develops its own dynamics and physics over the area of interest, far from domain boundaries. The focus region for evaluation and analysis is then a 200 km × 200 km square centred on the city of Paris (Figure 1, right).

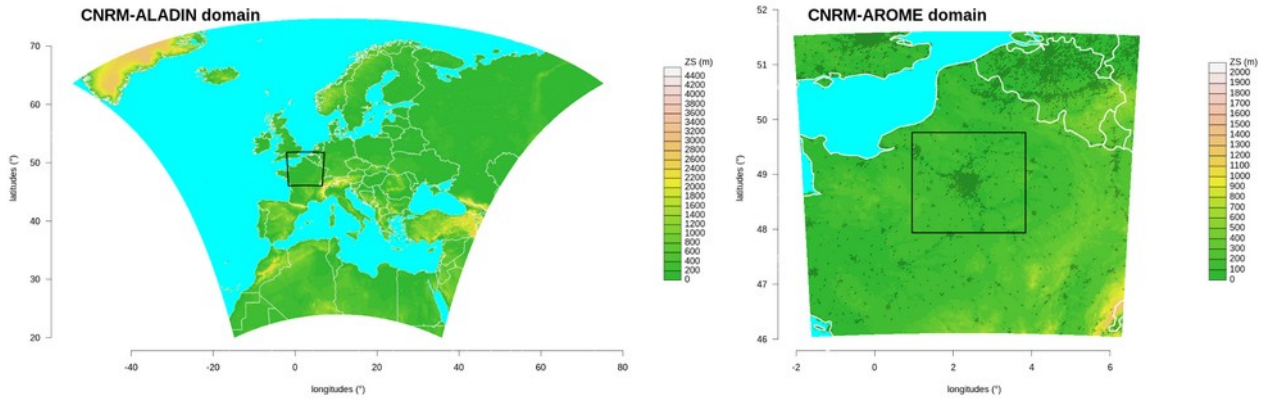

Figure 1: Presentation of the simulation domains for CNRM-ALADIN (left) and CNRM-AROME (right). The black rectangle on the left map is the CNRM-AROME domain, and the black rectangle on the right map indicates the boundaries of the study area.

2.2 Presentation of CNRM-ALADIN and CNRM-AROME climate models

CNRM-ALADIN is a limited-area regional climate model that covers horizontal resolutions of 10-50 km depending on applications. It is based on the hydrostatic assumption, a semi-Lagrangian advection scheme, and a semi-implicit time discretization for solving equations. Here, the model is used in its latest version 6.3 which main parameterizations for atmospheric processes (e.g. deep convection, turbulence, radiation, microphysics) are described by Nabat et al. (2020). Our case study is based on a CNRM-ALADIN6.3 configuration with 12. 5 km horizontal resolution and 91 vertical levels from 10 m to 1 hPa (hereafter referred to as CNRM-ALADIN), run for the EURO-CORDEX initiative (Jacob et al. 2014).

CNRM-AROME is a climate run version of the Météo France numerical weather prediction (NWP) AROME model (Seity et al. 2011; Brousseau et al. 2016), initially implemented and tested by Déqué et al.

(2016). With a horizontal resolution of 2.5 km, it is non-hydrostatic and it explicitly resolves the deep convection unlike CNRM-ALADIN, which makes it one of the high-resolution regional climate models known as CP-RCM. Its vertical grid is 60 levels from 10 m to 1 hPa. Although the total number of levels is lower than CNRM-ALADIN, the grid is more finely resolved in the lower atmosphere (with 27 levels up to 3000 m against 20 levels for CNRM-ALADIN) to better resolve surface-atmosphere interactions and atmospheric boundary layer processes. The version used here is equivalent to the earlier 41t1 cycle of the NWP model (Termonia et al. 2018) and already implemented for the simulations of the CORDEX Flagship Pilot Study (FPS) on Convection (see Caillaud et al. 2021 and Lucas-Picher et al. 2022 for more details). Concerning the CNRM-AROME configuration, preliminary tests and modifications have been made specifically for this study to adapt the settings of some parameterizations, and reduce some biases especially for incoming solar radiation. The radiative properties of clouds have been modified based on the operational version of the AROME NWP model. In addition, sensitivity tests on the cloud scheme led to a better tuning of the condensation threshold for undersaturation conditions, which resulted in an improvement of cloud cover simulation and of the resulting incoming radiation.

Both models are coupled to a surface module described in more detail in the next section.

2.3 Land surface modeling system

The NWP AROME model has been coupled since it was put into operation to the land surface modeling system SURFEX (Masson et al. 2013). SURFEX includes surface parameterizations dedicated to four different land cover types, i.e. seas and oceans, inland water (lakes and rivers), natural soils and vegetation, and urban areas.

More specifically, natural areas are treated with the Interaction Soil-Biosphere-Atmosphere (ISBA) model (Noilhan and Planton 1989, Boone et al. 1999). It resolves the radiation, energy, and water exchanges between a composite ground-based compartment that mixes soil and plant canopy, and the atmosphere. It also deals with the water and heat transfers in the soil column with three layers for water and two for temperature, and simulates the evolution with time of soil water content and soil temperature. For urban areas, SURFEX enables the activation of the Town Energy Balance (TEB) urban canopy model in a configuration close to its historical version (Masson 2000). TEB here treats exclusively the built-up fraction of the city based on the concept of an idealized urban canopy. The urban areas covered by a modeling grid point are described by a mean single canyon (but with multiple orientations) composed of a road with two vertical walls of equal height and a flat roof. Each element has its own materials with associated thermal and radiative properties, and the canyon is characterized by an average height and surface density of walls. TEB simulates separately for the road, the walls and the roof both radiation, energy, and water balances, then derives aggregated energy, water and momentum fluxes at the top of the urban canopy. At each grid point of the simulation domain, the surface fluxes are calculated by each model depending on the type of land use land cover, and then averaged as a function of the respective cover fractions in order to provide the surface conditions as input fluxes to the first atmospheric level of the AROME model. Note that the interface between SURFEX and CNRM-AROME is at the top of surface canopies without the atmospheric levels of CNRM-AROME penetrating within the urban and vegetation canopies.

For the climate simulation, some adjustments have been made to the CNRM-AROME version. The TEB model is here coupled to the Surface-Boundary-Layer (SBL) parameterization (Hamdi et al. 2007; Masson and Seity 2008) which allows to explicitly calculate the vertical exchanges of heat, humidity, momentum, and turbulent kinetic energy in the air volume within the urban canyon. This air volume is discretized in vertical layers from the ground surface to the first atmospheric level of CNRM-AROME located 10 m above the top of the urban canopy. The evolution of meteorological variables in each layer takes into account the contributions from heat and humidity turbulent fluxes and the drag effects of the vertical and horizontal urban surfaces present. The vertical mixing is resolved with a turbulent scheme and a parameterized mixing

length (Lemonsu et al. 2012). TEB thus explicitly calculates the air temperature at 2 m above the ground. The same SBL parameterization is applied for ISBA (Masson and Seity 2008) to discretize the atmospheric layer between the nature compartment and the lower level of CNRM-AROME. As a result, for mixed grid points combining built-up and natural covers, an averaged 2-m air temperature is diagnosed from those calculated separately by TEB and ISBA.

The CNRM-ALADIN model is also coupled to the SURFEX land-surface modelling platform but does not use the same configuration. For natural covers, the ISBA model is run in its diffusive version (ISBA-DF, Boone et al. 2000; Decharme et al. 2011). Cities are simply represented as rocky covers with high surface roughness, but without activating the dedicated urban model TEB.

2.4 Land use land cover database and physiographic data

For the CNRM-AROME configuration, the land uses and land covers are mapped with the global database ECOCLIMAP I (Champeaux et al. 2005) at 1-km spatial resolution. It consists of 243 classes including 11 urban classes. ECOCLIMAP I assigns to each class descriptive parameters i.e. the land use fractions and the surface properties required to prescribe the input data of the different SURFEX's surface models.

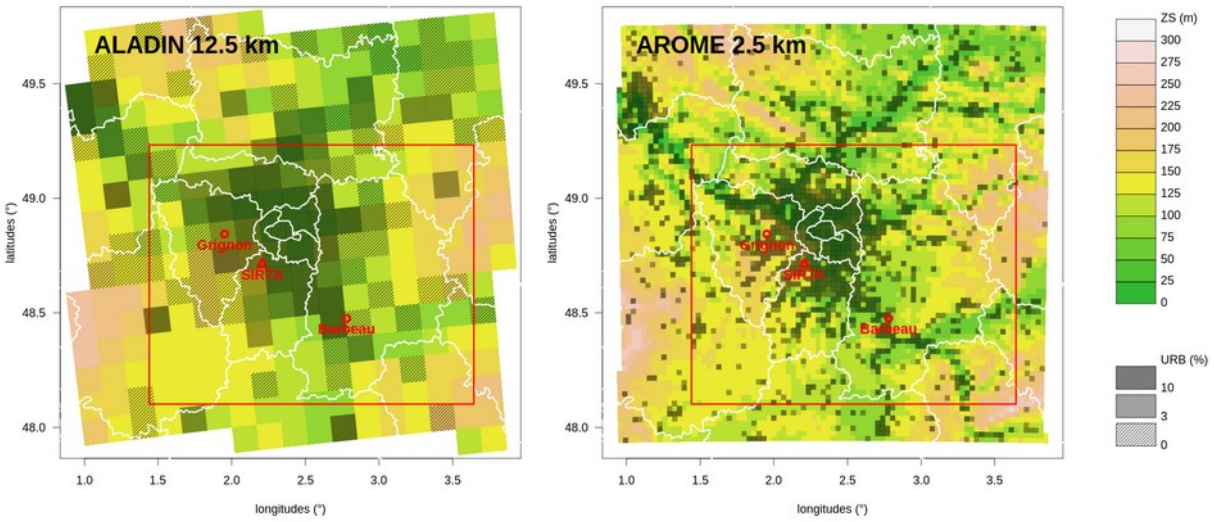

Figure 2: Comparison of ALADIN and AROME grids for the study domain. The color scale refers to the orography and the hatched areas are the urbanized grid points. The symbols indicate the location of the ICOS network flux stations (red circles) and the SIRTA site (red triangle). The red rectangle delineates the area of comparison to spatialized observations of TN/TX.

For natural areas treated with ISBA, the main parameters are soil and vegetation albedo, vegetation coverage fraction, vegetation height, leaf area index, and stomatal resistance. For urban classes, ECOCLIMAP I first describes each of them as a combination of built and natural surfaces. The nature part (which corresponds in reality to vegetation in the urban space) is treated independently by ISBA. The built-up part is described as a mean urban canyon with the associated parameters required by TEB, i.e. building density, average building height, wall surface density, as well as reflective properties, heat capacity, and thermal conductivity for materials of road, walls, and roof. As an example, the class "dense urban" is composed of 90 % of built-up areas and 10 % of natural areas. The buildings are 25 m high, with street aspect ratios of 0.83 and a building density of 45 %. Other urban classes mainly include "suburban areas", "commercial and industrial areas", "airports", "leisure areas", and some other minor classes. The ECOCLIMAP I data are projected onto the lower resolution CNRM-AROME grid, thus describing the composition of each grid point by fractions of land use land cover classes and resulting averaged surface parameters.

5

The relief is defined from the GMTED2010 (Global Multi-resolution Terrain Elevation Data) database provided by the U.S. Geological Survey (USGS) and the National Geospatial-Intelligence Agency (NGA) with a 250 m spatial resolution (Carabajal et al. 2011).

Figure 2 compares over the evaluation domain the effects of horizontal resolution of the two RCMs on the description of local topography and land use land cover mapping. The Paris Metropolitan area is located in a geologic basin with a weak relief. Depending on the resolution of the models, the relief varies from 52 to 239 m for CNRM-ALADIN, and from 6 to 284 m for CNRM-AROME with a little more spatial variability. Overall, the land cover land use distribution are comparable between the two models: the study subdomain of CNRM-AROME is composed of 6 % urban areas, 76 % crops and 17 % of forests, when the subdomain of CNRM-ALADIN is composed of 5% urban, 79 % crop, 11 % forest and 5 % of herbaceous areas. Nonetheless, the fine resolution of the CNRM-AROME grid makes it possible to better define the valleys and plateaus, as well as the spatial pattern of urbanized areas, than the CNRM-ALADIN grid.

3. Observational dataset for evaluation

3.1 Spatialized observations of precipitation and temperature

The monitoring of urban phenomena over long periods of time and the availability of suitable data for the evaluation of urban climate models at climatological scales is a real challenge. A study was conducted in the Paris region to collect, process and analyze long time series of spatialized data at kilometric resolutions of surface temperatures, near-surface air temperatures and precipitation (Le Roy et al. 2020). These data allowed the calculation of specific urban climate indicators to quantify the seasonal impact of urban areas on meteorological variables in relation to the local environment. For the present study, the evaluation of the CNRM-AROME climate model is based on two of the data sets for precipitation and air temperature.

The COMEPHORE product (Tabary et al. 2012) is a re-analysis of cumulative rainfall, gridded at 1 km horizontal resolution and with an hourly time step over Metropolitan France. It comes from the fusion of the radar reflectance measurements of the 24 radars of the French network and data from the rain gauge network. This product has been available since 1997. It is here used for the time period 2000-2017.

A specific gridded product of observed daily minimum and maximum temperatures (TN and TX) is provided for the Ile-de-France administrative region (including Paris Metropolitan area) since 2000. The data recorded by the stations of the Météo France's operational network are spatially interpolated with a horizontal resolution of 1.25 km (Kounkou-Arnaud and Brion 2018). The statistical method applies a linear regression and a spatialization of residues by kriging, by taking into account the relief variations, as well as the mapping of urbanization fraction coming from the land use database ECOCLIMAP (Faroux et al. 2013). This approach makes it possible to compensate for the lack of urban weather data and better capture the UHI pattern, especially along urbanized valleys. Hereafter, this product is referred to as IDF-TNTX.

3.2 Surface stations for global incoming radiation

Three flux measurement stations were located in the study area (see Figure 2) and provided global shortwave and longwave incoming radiation data for model comparison. Two of these stations are part of the international ICOS (Integrated Carbon Observation System) network: Grignon station installed in large cropland field and operational from 2004 to 2014, and Barbeau station located in a forest environment (with dominant oak and hornbeam in the understory) operating from 2005 to 2014. In addition, the academic atmospheric observatory of the SIRTA (Haeffelin et al. 2005), located in a suburban area to the south of Paris, provided a long-serie of radiation fluxes continuously from 2003.

3.3 Method of comparison to models

For the purpose of comparison with the model outputs, the two spatialized data sets of precipitation and temperature were projected onto the grid of the CNRM-AROME simulation domain with a 2.5-km horizontal resolution, thus degrading the initial horizontal resolution. The same process was done for the CNRM-ALADIN 12.5-km grid. Beforehand, the hourly precipitation data were aggregated to daily time step for comparison. For the radiation data, single grid point comparisons were made, i.e. by retrieving the simulated data at the CNRM-AROME grid points centred closest to the location of the three stations. Both observed and modelled radiation data were aggregated to daily time step and the three locations data were averaged together. Some statistics have been calculated seasonally for the time period 2000-2017 that is the longest period common to the available data. The standard deviation (Sdev), the mean bias (Bias), and the root-mean square error (Rmse) were calculated over the study domain as a whole for daily precipitation and temperature, and for the relevant grid points for radiation.

4. General evaluation of CNRM-AROME over Paris regional

In a first step, CNRM-AROME is evaluated in a general way to qualify its capability to simulate the environmental conditions at the regional scale (here for the study domain). The evaluation covers daily precipitation, short- and longwave incident radiation, and near-surface minimum and maximum daily temperatures. We are also interested in the possible added-value of the CNRM-AROME model compared to the CNRM-ALADIN 12.5 km resolution driver model.

4.1 Daily rainfall

The daily precipitation rates derived from the COMEPHORE reanalyses are projected both on the CNRM-AROME 2.5-km resolution grid and the CNRM-ALADIN 12.5-km resolution grid, and then compared to model outputs in the form of monthly rainfall averaged over the domain (Table 1). CNRM-AROME daily rainfall presents a strong overestimation from October to May with maximum bias in MAM (+1.09 mm day-1), associated with too many wet days at this period, when rainfall are correctly simulated from July to September. Comparable trends are noted for CNRM-ALADIN simulations but biases are weaker (less than 0.7 mm day-1). On the contrary, both daily rainfall and number of wet days are underestimated in JJA by CNRM-ALADIN. At this time of year when convective precipitation events are more frequent, CNRM-AROME appears to provide an improvement over CNRM-ALADIN. This could result from the explicit resolution of deep convection and better dynamics in accordance with previous studies of Fumière et al. (2020) and Caillaud et al. (2021).

Table 1: Mean seasonal bias in daily rainfall and mean seasonal percent bias in number of wet days (for daily rainfall ≥ 1 mm) calculated for both the CNRM-AROME and CNRM-ALADIN models with respect to the observational product COMEPHORE.

	Bias RR24 (mm day-1)				Bias number of wet days (%)			
	DJF	MAM	JJA	SON	DJF	MAM	JJA	SON
CNRM-AROME	+0.74	+1.09	0.	+0.61	+9.05	+11.96	-0.19	+6.00
CNRM-ALADIN	+0.53	+0.67	-0.42	+0.25	+9.64	+9.07	-4.10	+4.05

4.2 Incoming radiation

The long- and shortwave incoming radiation simulated by CNRM-AROME and CNRM-ALADIN are compared to the data of the three flux stations (see Section 3.2) through monthly averages calculated for the common 2000-2017 time period. For CNRM-AROME, a slight underestimation of the incoming longwave

radiation is noted in winter and more particularly in spring (April and May) with mean biases of -2.4 and -7.6 W m^{-2} in DJF and MAM, respectively (Figure 3, left). On the contrary, the incoming shortwave radiation is overestimated by +4.5 W m^{-2} in JJA. Comparing these results to those of CNRM-ALADIN, it is noted that CNRM-AROME much better performs than CNRM-ALADIN which systematically overestimate the incoming shortwave radiation with seasonal variations from 8% in DJF to nearly 35% in JJA (which represents in this case a bias of more than 50 W m^{-2}). The improvement obtained in the CNRM-AROME simulation compared to CNRM-ALADIN is mainly due to the improvement of the cloud scheme (see Section 2.2) which allows to better represent the cloud cover for undersaturated atmospheric conditions especially in summer period. This defect is a fairly well-known bias in regional climate models and was highlighted by Lucas-Picher et al. (2022) for CNRM-AROME in its standard version.

The incoming longwave radiation is mainly overestimated from December to April (that could be in accordance with too many clouds) but with biases not exceeding 5%. It compares well with the measured fluxes for the other months of the year (Figure 3, right). Note that for incoming longwave radiation, CNRM-ALADIN has very good scores with maximum seasonal bias of 1%.

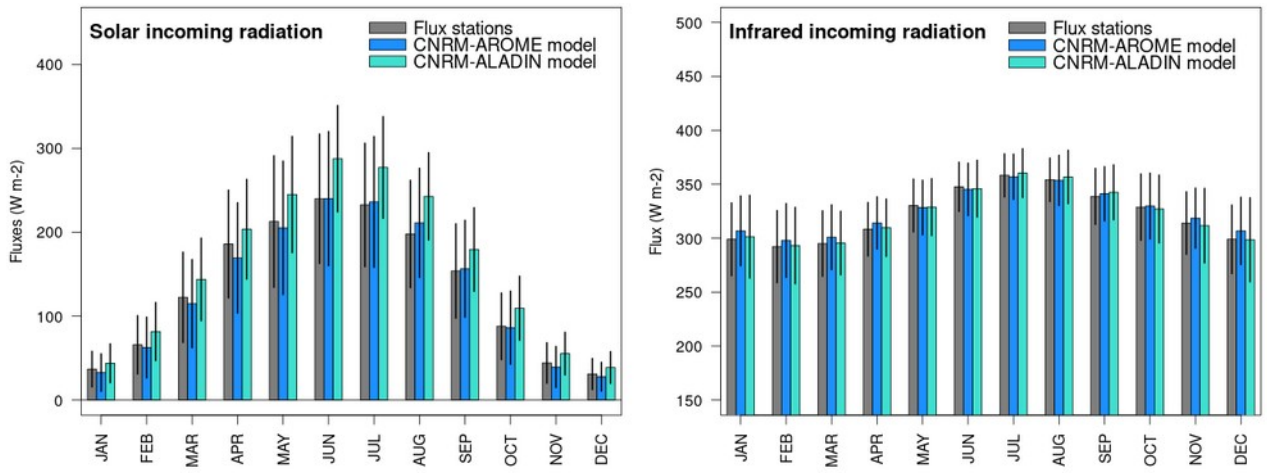

Figure 3: Comparison of monthly solar and infrared incoming radiation calculated from the fluxes measured at the three stations (SIRTA, Barbeau, Grignon) and averaged, and simulated at the corresponding grid points with CNRM-AROME and CNRM-ALADIN and averaged.

4.3 Near-surface air temperature

TN and TX maps from IDF-TNTX database are projected both on CNRM-AROME 2.5-km grid and CNRM-ALADIN 12.5-km grid for comparison over time period 2000-2017. For a fair comparison between models, the CNRM-AROME TN and TX are also projected onto the CNRM-ALADIN grid.

CNRM-AROME overestimates TN whatever the season, but with a noticeable variability in time. As indicated in Table 2, Bias and Rmse are minimum in MAM (+0.83 and 2.92°C, respectively) and maximum in JJA (+1.72 and 3.55°C). Overall, the maps of seasonal bias (CNRM-AROME minus IDF-TNTX) have very little spatial discontinuity between the urban area and the rest of the domain, contrary to what is found for CNRM-ALADIN. The model performs quite well for the Paris urban area, where biases do not exceed 0.5-1.5°C. Nonetheless, an area of broadleaf forest south-southeast of Paris that is noted systematically warmer in the simulation for both models (Figure 4), that could result from soil or surface properties. Especially, the soil texture database HWSD (Harmonized World Soil Database, Nachtergaele et al. 2012) that feed the ISBA model maps a very sandy soil in this area (not shown), consequently the soil is there more draining and with a higher heat capacity.

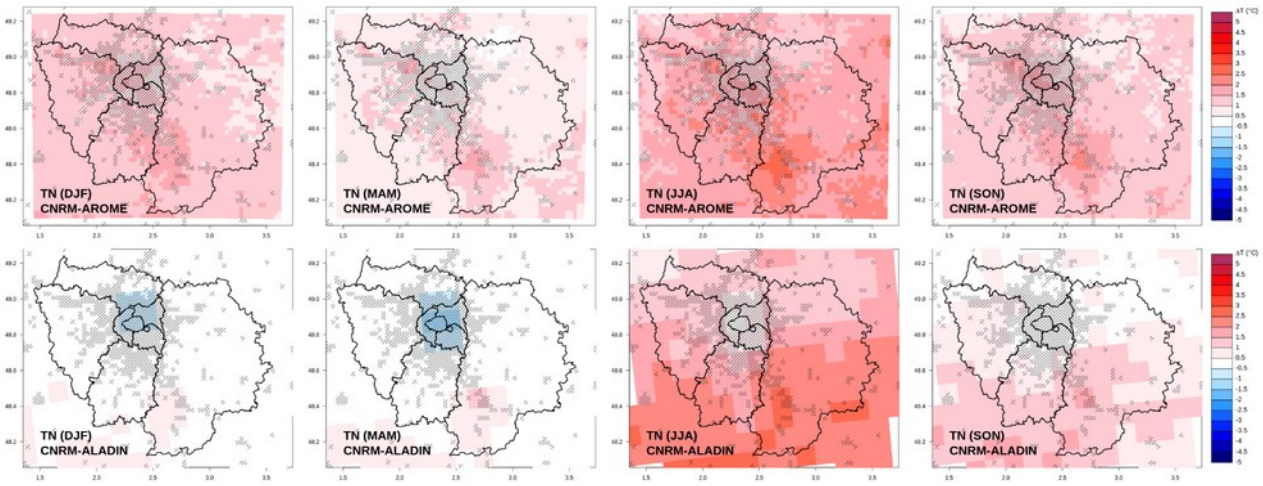

Figure 4: Comparison of seasonal bias maps in TN calculated over the time period 2000-2017 between both CNRM-AROME (top) and CNRM-ALADIN (bottom) simulations and the reference IDF-TNTX database. Hatching represents the extent of Paris urban area (with a cover threshold of 10 % of the CNRM-AROME grid cells, according to the ECOCLIMAP database).

Contrary to TN, the CNRM-AROME Bias is systematically negative for TX. It is less than 1°C for DJF, JJA and SON, indicating very good average model performance (Table 2). Nevertheless, the Rmse is 4.18 °C in JJA, which results from a discrepancy in the representation of the interannual variability of summer TX. The main defect is noted in MAM during which the rainfall excess results in a strong underestimation of TX by -2.0°C on average. Finally, biases tend to be slightly lower in the city compared to the surrounding crops and forest areas (Figure 5) where the evapotranspiration response of natural areas is strongly governed (and enhanced in this case) by water inputs coming from rainfall.

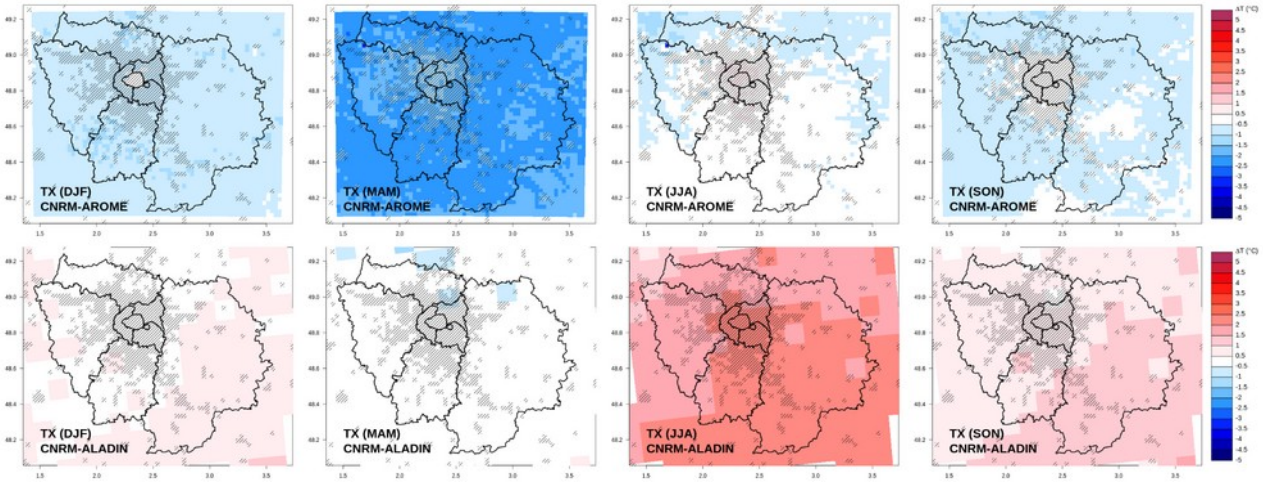

Figure 5: Same than Figure 4 for TX.

In view of Bias scores, the added value of CNRM-AROME compared to CNRM-ALADIN is not clear regarding domain-average temperatures (Table 2). The differences are small but the Bias is better with CNRM-ALADIN, except in JJA for TN and JJA-SON for TX. Nevertheless, the comparison of simulated versus observed standard deviations and of Rmse are rather in favour of CNRM-AROME, which seems to suggest that the TN/TX spatial variability is better simulated with the higher resolution. This point on the spatial variability of the simulated fields with both models is discussed in more detail in Section 5.1 related to urban effects.

The general evaluation of CNRM-AROME highlights some weaknesses in the simulation of precipitation (especially during spring), when incoming radiation is quite acceptably simulated. The near-surface temperatures are nonetheless correctly simulated both for nighttime and daytime. The main shortcoming is a daytime cold bias (TX) in MAM in response to excess wet days. The added value of CNRM-AROME on the spatial-averaged fields is not clearly demonstrated. However, the contribution of the resolution comes into play in the representation of the spatial variability of these fields. This finding is confirmed in the following.

5. Urban climate modeling capability

In a second stage, the objective is to investigate the capability of CNRM-AROME to simulate the specificities of the urban climate of the Paris region, at the seasonal scale and also at the event scale. This analysis is for a large part based on the urban climate indicators proposed by Le Roy et al. (2020) from the processing of long-term time series of spatialized observations available over the study area, especially for air temperature and UHI, and for precipitation.

Table 2: Seasonal Bias and Rmse in TN and TX calculated for both the CNRM-AROME and CNRM-ALADIN models with respect to the observational product IDF-TNTX. For CNRM-AROME, these statistics are calculated on the native CNRM-AROME grid and after projection on the CNRM-ALADIN grid. The standard deviation of each dataset is also given.

			DJF		MAM		JJA		SON	
			(2.5 km)	*(12 km)*	*(2.5 km)*	*(12 km)*	*(2.5 km)*	*(12 km)*	*(2.5 km)*	*(12 km)*
TN (°C)	IDF-TNTX	Sdev	4.31	4.31	4.20	4.18	3.06	3.05	4.44	4.43
	CNRM-AROME	Sdev	3.74	3.76	4.00	3.97	4.00	3.97	4.66	4.64
		Bias	+1.24	+1.25	+0.83	+0.85	+1.72	+1.72	+1.21	+1.21
		Rmse	2.95	2.95	2.92	2.91	3.55	3.53	3.09	3.07
	CNRM-ALADIN	Sdev	-	3.76	-	4.09	-	4.05	-	4.97
		Bias	-	+0.18	-	+0.10	-	+1.81	-	+0.80
		Rmse	-	2.86	-	2.88	-	3.73	-	3.26
TX (°C)	IDF-TNTX	Sdev	4.08	4.07	5.20	5.20	4.36	4.36	5.69	5.69
	CNRM-AROME	Sdev	3.48	3.48	4.53	4.52	5.78	5.77	6.56	6.55
		Bias	-0.81	-0.79	-2.02	-2.01	-0.29	-0.31	-0.61	-0.61
		Rmse	2.60	2.58	3.62	3.61	4.18	4.16	2.93	2.91
	CNRM-ALADIN	Sdev	-	3.45	-	5.09	-	5.89	-	6.68
		Bias	-	+0.47	-	-0.23	-	+1.98	-	+0.93
		Rmse	-	2.64	-	2.99	-	4.52	-	3.11

5.1 Urban heat island

Using the spatialized TN and TX data, and a land use mask to separate urban and rural areas, Le Roy et al. (2020) proposed two indicators to qualify the UHI. The first one is the intensity of UHI (I_{UHI}), which is the difference between the temperature averaged over urban areas and the temperature averaged over rural areas. It is calculated both for nighttime and daytime based on TN and TX, respectively. The second is the temperature extent of UHI (TE_{UHI}), which is the fraction of the total urban area affected by a minimum UHI intensity. It is calculated for UHI intensity thresholds (from 0.5 to 5 K) and both for nighttime and daytime.

10

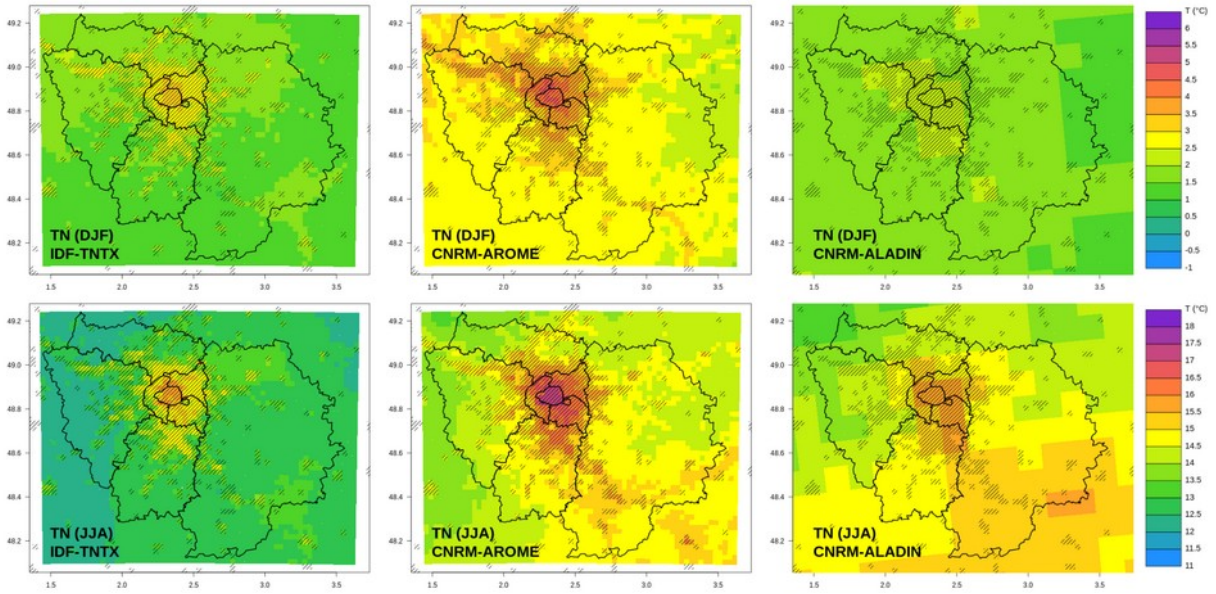

Figure 6: Comparison of seasonal mean maps in TN (for DJF and JJA) calculated over the time period 2000-2017 from the IDF-TNTX database and from both CNRM-AROME and CNRM-ALADIN simulations. Hatching represents the extent of Paris urban area (with a cover threshold of 10% of the CNRM-AROME grid cells, according to the ECOCLIMAP database).

Nighttime UHI

The TN maps for both DJF and JJA show that the UHI phenomenon has a spatial pattern that follows the urbanized areas that preferentially extend along valleys (Figure 6, left). The maximum values in TN are observed in the Paris centre and they decrease progressively with the urbanization rate. In the background, the temperatures of the natural areas have some variability with respect to land use and regional temperature gradients. The UHI indicators deduced from this are presented in Figure 7 (top left). Intensities of UHIN deduced from spatialized observations are systematically positive. They are greater between April and September, and reach a maximum in June. The seasonal statistics indicate that I_{UHIN} reaches 1.56°C on average and 2.80°C as the 90th quantile in JJA (Table 3). The intensity decreases between October and March, when meteorological conditions are less favorable (less radiation, more wind, more precipitation). Nonetheless, the persistence of a winter UHIN is noted with an I_{UHIN} of 0.92°C (1.73°C) in average (90th quantile) in DJF, that partially results from heat release by heating equipment. The spatial extension TE_{UHIN} also shows seasonal variability (Figure 7, bottom left). For example, based on a threshold of 1.5°C, it can be seen that nearly 40 % of the city is affected between April and September, compared to about 20 % during the rest of the year.

Table 3: Comparison of seasonal daytime and nighttime UHI intensities calculated over time period 2000-2017, from the IDF-TNTX observation product, and both CNRM-AROME and CNRM-ALADIN simulations.

		DJF		MAM		JJA		SON	
		Mean	*(Q90)*	*Mean*	*(Q90)*	*Mean*	*(Q90)*	*Mean*	*(Q90)*
I_{UHIN}	IDF-TNTX	0.92	(1.73)	1.39	(2.56)	1.56	(2.80)	1.12	(2.19)
	CNRM-AROME	0.81	(1.29)	1.26	(2.15)	1.60	(2.57)	1.24	(2.11)
	CNRM-ALADIN	0.30	(0.85)	0.77	(1.58)	0.94	(1.74)	0.35	(0.93)
I_{UHIX}	IDF-TNTX	0.71	(1.39)	0.56	(1.22)	0.19	(0.88)	0.40	(1.08)
	CNRM-AROME	0.83	(1.28)	1.14	(1.77)	1.25	(2.11)	0.89	(1.51)
	CNRM-ALADIN	0.23	(0.66)	0.64	(1.28)	0.83	(1.48)	0.37	(0.98)

CNRM-AROME simulates a quite realistic climatology of UHIN. The seasonal TN maps show spatial

patterns in very good agreement with the observed maps despite a slightly warm bias across the domain (Figure 6, middle), and as shown in Figure 4, both the averages and the seasonal extremes of I_{UHIN} are very similar to those observed. The model correctly simulates the high intensities of summer I_{UHIN} and up to September, and the persistence of winter I_{UHIN} (Figure 7, top middle). However, it slightly underestimates the I_{UHIN} over the transition period of April-May, as well as the monthly variance throughout the year that results from the day-to-day variability of the phenomenon as a function of weather conditions. The same findings are obtained when comparing the indicators of observed and simulated spatial extension (Figure 7, bottom middle). The seasonal TN maps retrieved from CNRM-ALADIN simulation are much smoother than that observed and simulated with CNRM-AROME, and the temperature anomaly of urban areas is less contrasted and less extended (Figure 6, right). This results from a less accurate description of land use due to the 12.5-km spatial resolution, combined with a more rough surface parameterisation. By simulating urban areas as rocky covers, CNRM-ALADIN globally underestimates the heat daytime storage and nighttime release capacity of the urban canopy, which leads to a nighttime cooling too fast in urban areas. The I_{UHIN} peak rises in June as in the observations but underestimated (Figure 7, right): for JJA, the mean value of I_{UHIN} and the 90th quantile are only 0.94 and 1.74°C, respectively (Table 3). The UHIN season is also shorter with significantly lower intensities from August to May. Averaged rural TN are comparable in both CNRM-AROME and CNRM-ALADIN simulations so that these differences noted in UHIN intensity and saisonality between models are driven by urban TN. The rapid weakening of UHIN in late summer in the CNRM-ALADIN simulation is related to less warming of rock surfaces. In winter, UHIN is very low in CNRM-ALADIN because anthropogenic heat discharges are not considered.

It is important to note that UHI indicators (as presented in Figure 7) were also calculated and compared by interpolating the IDF-TNTX and CNRM-AROME data onto the CNRM-ALADIN 12.5-km resolution grid, and the conclusions remained unchanged.

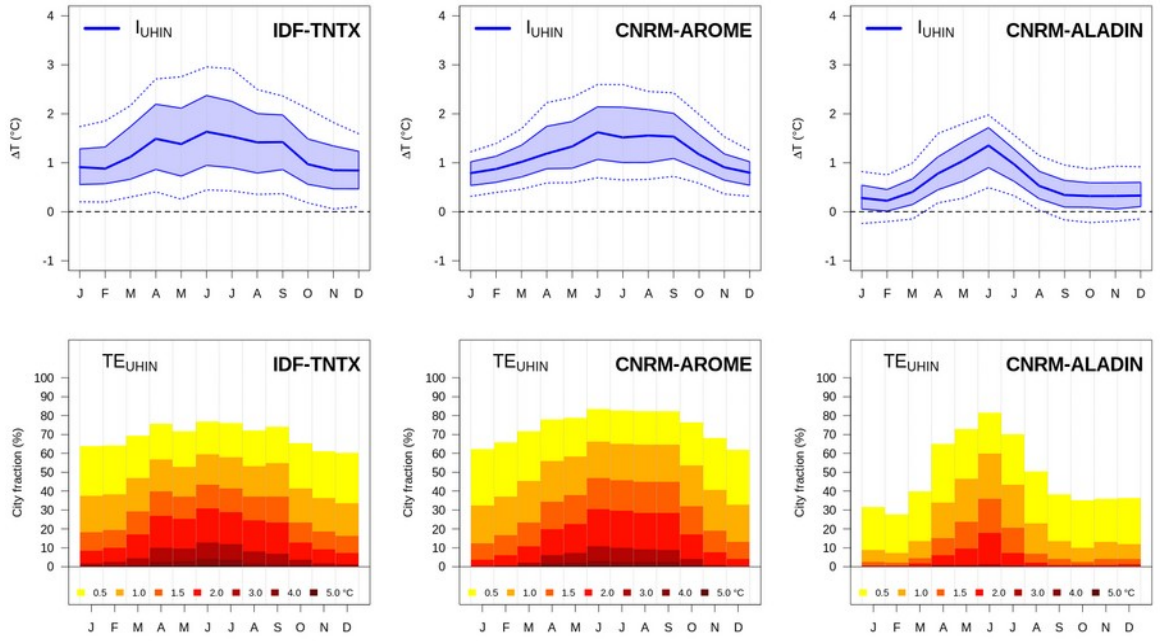

Figure 7: Comparison of monthly indicators I_{UHIN} (top) and T_{EUHIN} (bottom) calculated from IDF-TNTX observations interpolated on the CNRM-AROME grid, and from both models CNRM-AROME and CNRM-ALADIN. For I_{UHIN}, the blue shaded area delimits the 25th–75th percentiles data range, and lower and upper dashed lines the 10th and 90th percentiles.

Daytime UHI

The UHI is known to be a preferentially nocturnal process as it results from a difference in cooling rates between the urban and surrounding natural areas. During the day, the seasonal TX maps from IDF-TNTX spatialized observations show slightly warmer temperatures along the urbanized valleys but combined with regional temperature contrasts (Figure 8, left). This results in less spatially structured and lower I_{UHIX}. The seasonality is reversed with respect to UHIN: I_{UHIX} is maximum in DJF (0.71 and 1.39°C in mean and 90th quantile, respectively) and minimum in JJA (0.19 and 0.88°C) (Figure 9 and Table 3).

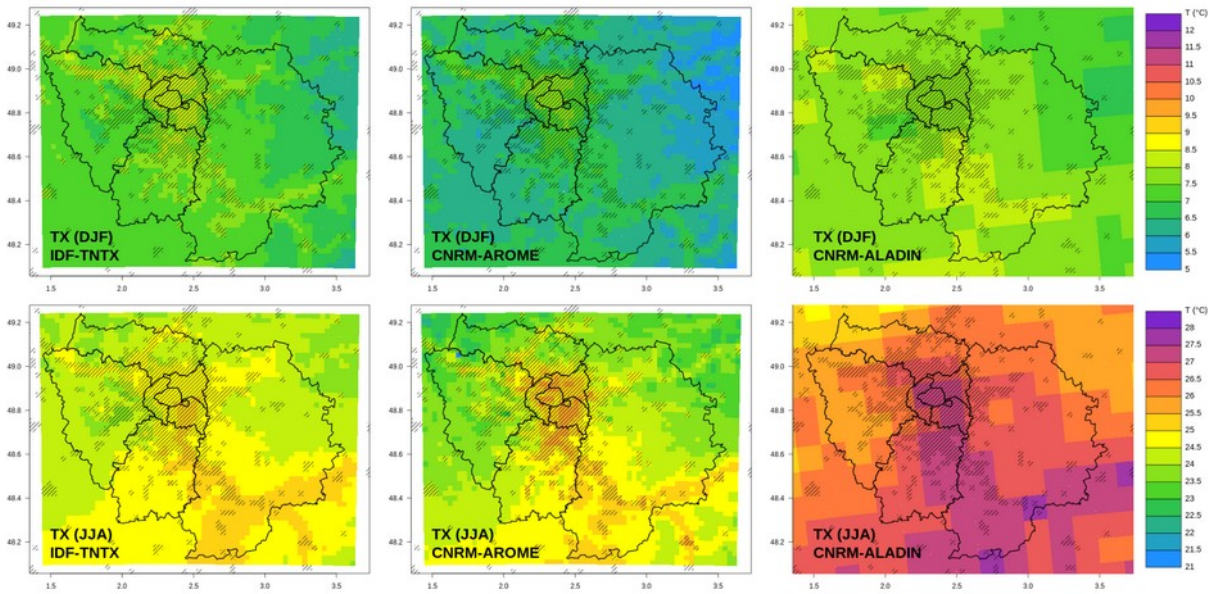

Figure 8: Same than Figure 6 for TX.

CNRM-AROME simulates TX map comparable to observations in DJF, but with a bit too strong urban/rural thermal contrast in JJA (Figure 8, middle). The seasonality is poorly captured with too high I_{UHIX}, especially in MAM and JJA (by 0.6-1°C on average, Figure 9 and Table 3). According to the previous général evaluation of TX (Figure 5), this defect mainly results from a too marked cooling in natural environments surrounding the Paris metropolitan area, whereas the temperature conditions are correctly simulated by CNRM-AROME in the city. CNRM-ALADIN shows a seasonality somewhat comparable to that of CNRM-AROME (i.e. minimum UHIX in DJF and maximum in JJA), but with overall lower intensities (Figure 8, left). As for nighttime, UHIX is very weak in winter and underestimated by CNRM-ALADIN.

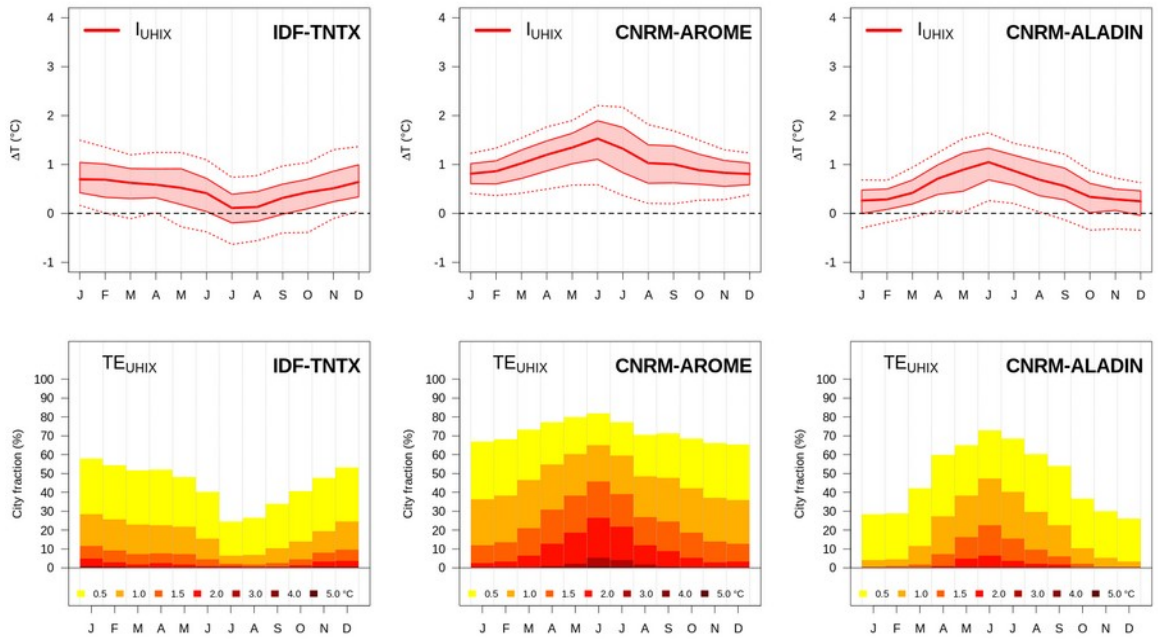

Figure 9: Same than Figure 7 for indicators I_{UHIX} (top) and TE_{UHIX} (bottom).

5.2 Heat-wave warning days

With a perspective to apply such simulations for impact studies in urban areas, a focus on summer temperatures is carried out here to assess the capacity of climate models to predict heatwave warning situations. The heat-wave index proposed by the French national Public Health Agency (Santé Publique France), in collaboration with Meteo France, regarding the heat-wave warning plan for population prevention is applied here. Time series to calculate the daily minimum and maximum biometeorological indices (BMIN and BMIX) were calculated as a three-day moving average (for days D, D+1, D+2) of TN and TX, respectively. A heat-wave peak is identified when both indices exceed the minimum and maximum temperature thresholds simultaneously. These thresholds were defined by the Public Health Agency, by administrative county (see counties in Figure 10, top left panel) and based on epidemiological analyses (Pascal et al. 2021, see supplementary material for detail). For Paris (county 75) and the inner suburbs (counties 92, 93, 94), the BMIN/BMAX thresholds are 21/31°C, respectively. They are 20/35°C for both counties 91 and 95, 18/34°C for county 77, and 19/33°C for county 78. The day D of the heat-wave peak is associated with the following two days D+1 and D+2 (used in the calculation of moving average), which makes it possible to match the days together to define a continuous heat-wave event whose minimum duration is three days by definition.

This heat-wave definition was applied to the IDF-TNTX observation product, and the same way to the TN/TX simulated by CNRM-AROME and CNRM-ALADIN, by grid points. The Figure 10 (top panel) shows the results as maps of the average number of heat-wave days per year for the period 2000-2017. According to the IDF-TNTX product, the Paris region experienced between 0 and 5 heat-wave days per year over 2000-2017 (Figure 10, top left). The spatial differences observed are partly governed by urbanization, with more frequent heat-wave warning days in Paris center and inner suburbs (75, 92, 93, 94). In addition, geographical variations exist between counties in second suburbs with the counties 77 and 95 having the most and least number of heat wave days, respectively. These contrasts are partly explained by the different thresholds set by SPF (BMIN threshold being lower for 77 than for other counties) but also by the temperature regional climatological gradient of temperature between south-east (hotter) and north-west (cooler) of the region as observed in Figure 6 and Figure 8.

Both models CNRM-AROME and CNRM-ALADIN greatly overestimate heat-wave conditions, by simulating up to 18 days per year in some areas (Figure 10, top middle and right). For CNRM-AROME, this overestimation results more significantly from biases in extremes of TN that are too warm compared to observations, when extremes in TX are more realistic. For CNRM-ALADIN, biases both in extremes of TN and TX are noted. Consequently the thresholds are frequently exceeded simultaneously for simulated BMIN and BMAX.

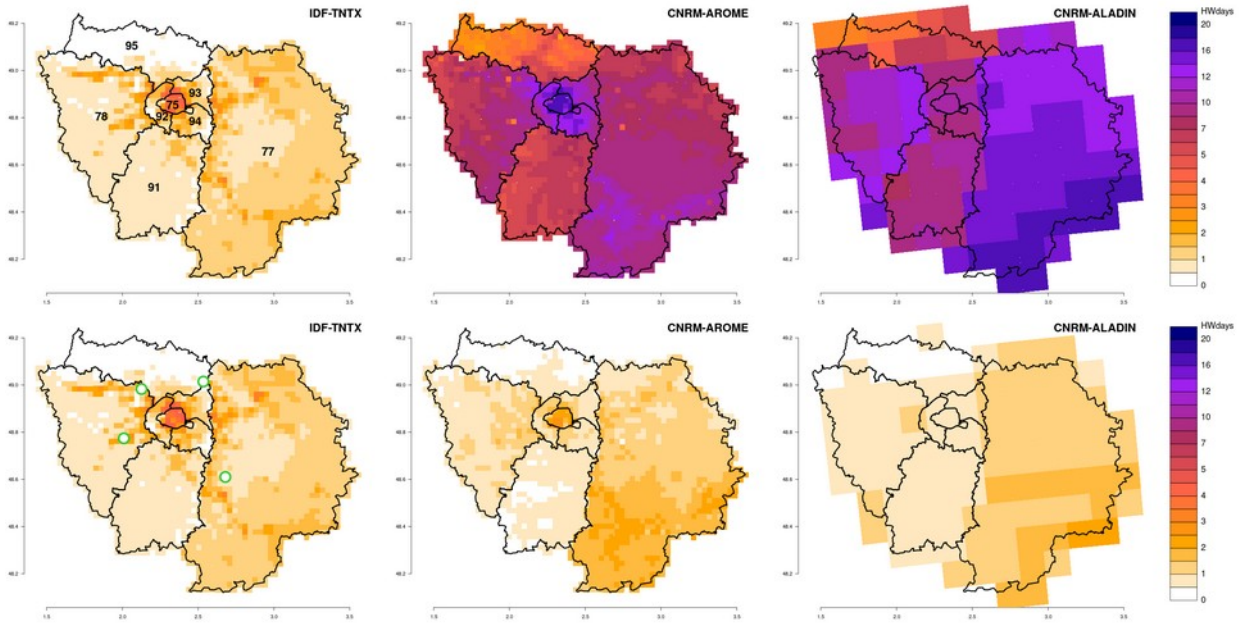

Figure 10: Maps of the average number of heat-wave days per year retrieved for time period period 2000-2017 from the IDF-TNTX observation product, and from the TN/TX simulated by CNRM-AROME and CNRM-ALADIN using the raw outputs (top), and after debiasing the models (bottom, with the green circles to locate the four stations used for quantile-quantile correction).

To overcome these biases, TN and TX of both models were debiased. Two reference observed time series were calculated over 2000-2017 for TN and TX, by averaging TN and TX time series from four stations of the Meteo-France operational network (Roissy, Melun, Trappes et Achères) spread across the region to the N, SE, SW, and NW, respectively. The same quantile-quantile correction over the whole simulation domain was applied to the simulated TN data, by climatological season (same for TX). With this correction, the number of heat-wave warning days is much more realistic (Figure 10, bottom). The geographical variability between counties is found overall, both with CNRM-AROME and CNRM-ALADIN. However, CNRM-AROME better represents the finer variabilities linked to urbanization, even if a slight underestimation is noted for Paris center and first suburbs.

5.3 Urban effects on local precipitation

The study by Le Roy et al. (2020), based on a long series of COMEPHORE observations, shows a trend in higher daily rainfall downwind than upwind of the Paris urban area. These results were obtained by comparing integrated daily rainfall over two geographical areas of equal size, one upwind of the city (control area) and one downwind of the city (under-influence area). These areas are two opposite sectors of the same 100-km radius circle centered on Paris, whose orientation is determined on a daily basis according to the mean wind direction. The excess of precipitation downwind is +25 % on average over the year i.e. +0.93 mm per day (as median value calculated for time period 2000-2017), but a substantial seasonal variability is noted: +29 % (+0.90 mm per day) in DJF, +23 % (+0.86 mm per day) in MAM, +27 % (+1.19 mm per day) in JJA, +21 % (+0.88 mm per day) in SON (Figure 11, left and Table 4).

15

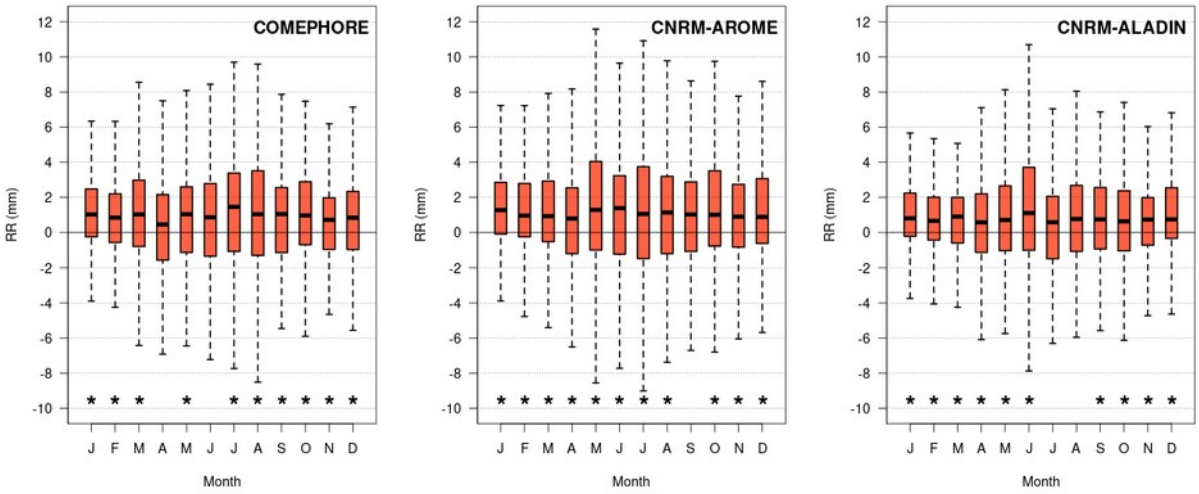

Figure 11: Comparison of monthly averages of daily precipitation rate differences calculated between the downwind and upwind areas of the city, calculated from COMEPHORE observations and modelling data from both CNRM-AROME and CNRM-ALADIN for period 2000-2017. Only wet days (daily rainfall ≥ 1 mm over at least one of the two sectors) are considered in the analysis. Asterisks indicate significant differences based on Student's t test with a 95% confidence interval.

For comparison, the methodology was also applied to precipitation data from CNRM-AROME and CNRM-ALADIN simulations over the same period. In the same way as for the COMEPHORE gridded data, the grids of CNRM-AROME and CNRM-ALADIN are both intersected with the upwind and downwind sectors, without modifying the native resolution of the models (2.5 and 12.5 km, respectively), in order to calculate the total daily precipitation in each sector depending on wind direction (Figure 11, middle and right). Both models simulate an excess of daily precipitation downwind of the city over the year, which is statistically significant in almost all months of the year, as in the observations. CNRM-AROME seems to better capture the intensity and the seasonal variability of the phenomenon than CNRM-ALADIN. The median values of seasonal and annual differences obtained comparing rainfall downwind and upwind of the city, for the observations and the two models, are presented in Table 4. The rainfall increase downwind is systematically underestimated in CNRM-ALADIN, and conversely is overestimated in CNRM-AROME (except in JJA) with less bias. On an annual scale, CNRM-AROME is better than CNRM-ALADIN, especially because of the good results in JJA and SON.

Table 4: Seasonal and annual differences (as median, in mm per day) between daily precipitation rates over the downwind and upwind areas of the city, calculated from COMEPHORE observations and from both CNRM-AROME and CNRM-ALADIN data for period 2000-2017. The value in brackets is the average increase in %.

	COMEPHORE mm day-1 (%)	CNRM-AROME mm day-1 (%)	CNRM-ALADIN mm day-1 (%)
All year	0.95 (25)	1.03 (28)	0.75 (21)
DJF	0.90 (29)	1.12 (38)	0.73 (27)
MAM	0.86 (23)	0.99 (23)	0.77 (21)
JJA	1.19 (27)	1.10 (25)	0.84 (18)
SON	0.88 (21)	0.94 (26)	0.72 (18)

According to scientific literature, urbanization may influence local precipitation through thermal and aerodynamic effects (Liu and Niyogi 2019). The UHI reflects an increase in air temperature in and above the

city that can induce local airflow circulations and enhance the humidity content in the atmosphere and saturation potential. In addition, the surface roughness of the urban canopy acts as a physical barrier on the synoptic flow, and can generate updrafts over the city. Depending on the synoptic wind conditions and UHI intensity of the day, the way these thermal and aerodynamic effects combine to influence precipitation varies. This could explain the seasonal variations observed (and simulated by CNRM-AROME) but would require further investigation and sensitivity analysis. Although expected seasonal variations are not represented, the results obtained with CNRM-ALADIN suggest that the model is able to simulate a certain influence of the city on precipitation, despite the horizontal resolution of 12.5 km and the simple parameterization applied to urban covers (strong surface roughness and heat capacity).

6. Conclusion

In view of the general evaluation of CNRM-AROME over the Paris region, based on mean climatological fields analyses, it seems difficult to state the added value of the CNRM-AROME compared to the regional climate model CNRM-ALADIN. Some systematic biases were noted, especially an excess of precipitation, both in terms of daily rainfall and number of wet days, which is particularly marked in spring. The biases were accentuated in comparison to those already noted in the CNRM-ALADIN simulation over the same domain. These findings are in line with those obtained for the largest EUCP domain covering northwestern Europe, that could result from an overly active deep convection in the CNRM-AROME CP-RCM as mentioned by Lucas-Picher et al. (2022). Concerning radiation forcing, Lucas-Picher et al. (2022) found an over-estimation of the incoming shortwave radiation in summer over continental areas (including Paris region) by both CNRM-AROME and CNRM-ALADIN. Here, a comparable bias has been also noted for CNRM-ALADIN, due to a cloud-cover underprediction, and for CNRM-AROME in its default configuration (not shown here). Forecasts over Metropolitan France by the NWP AROME model present this fairly recurrent bias, linked to a lack of clouds. We suspect that this is the result of the PMMC09 shallow convection scheme (based on Pergaud et al. 2009) which tends to be too active at the inversion level for stratocumulus cases and to disrupt their diurnal cycle. Nonetheless for the present study case, better performances have been achieved for CNRM-AROME by adapting the condensation threshold applied in the cloud scheme for undersaturation conditions.

The daytime near-surface air temperatures simulated by CNRM-AROME and CNRM-ALADIN are obviously influenced by the realism or defect of these atmospheric conditions, and through the modeling of surface processes that govern the heat and water vapor exchanges with low-level atmosphere. As a consequence of previous findings, the clearest differences between the two models were noted in summer and spring over natural areas. In summer, TX is much warmer in CNRM-ALADIN simulation due to excess in solar radiation, and therefore more pronounced surface heating and heat convective exchange. In spring, TX is much colder in CNRM-AROME simulation as a response of too wet conditions that results in strong cooling by evapotranspiration from natural soil and vegetation. For nighttime temperature TN, the difference between model performances are mostly related to the differences in surface properties description (and associated horizontal resolution) and in physical parameterizations. The spatial temperature variability related to the relief is more finely represented in CNRM-AROME. Furthermore, the absence of a specific urban surface scheme in CNRM-ALADIN results in a systematic cold bias over urban areas.

A more specific analysis of these urban effects clearly highlights the added-value of the CNRM-AROME model for the simulation of realistic UHI compared to CNRM-ALADIN. The spatial pattern and the intensity of nighttime UHI, as well as the seasonal variability of the phenomenon, are much better captured with CNRM-AROME, thanks to the finer horizontal resolution and to the inline implementation of the TEB urban canopy model. The possible impact of urban areas on precipitation and its seasonal variability (in line with what was observed by Le Roy et al. 2020) also appear to be better represented.

Finally, a high-resolution regional climate model such as CNRM-AROME, with specific modeling of urban

surface processes, is a promising tool to diagnose climatic and impact indicators at the city scale, and their evolutions in a changing climate. A multi-city assessment in Metropolitan France also confirms these results for the nighttime urban heat island (Michau et al. 2022). For the present evaluation, nevertheless, the indicators associated with extreme heatwave events (and calculated on the basis of prescribed temperature thresholds being exceeded) are overestimated when calculated from raw model outputs. A quite simple adjustment made it possible to significantly improve the results, which raises the question of simulation debiasing for calculation of impact indicators.

Nevertheless, some ways can be investigated to improve the current physical parameterisations of CNRM-AROME, which has so far been applied mainly to study Mediterranean convective rainfall events (Fumière et al. 2020; Caillaud et al. 2021). Work is currently in progress (especially for the NWP version of AROME) on the microphysical parameterisations, the radiative scheme, and the shallow-convection scheme. A finer vertical resolution of the atmosphere is also considered and has been shown to be useful in modelling fog events (Philip et al. 2016). Moving to an even finer horizontal resolution has also shown improvements (1.3 km compared to 2.5 km for the NWP AROME model, Brousseau et al. 2016) but this option is not considered for now for climate configuration. Some developments are also planned for surface processes. The new CNRM-AROME cycle, combined with an updated version of the SURFEX land surface modeling system, will make it possible to test new configurations for both TEB and ISBA models. Especially for cities, the benefit of modeling urban vegetation (Lemonsu et al. 2012) and building energy functioning (Pigeon et al. 2014) will be tested.

Acknowledgements The AROME model is developed from a collaboration between CNRM and CNRS laboratories involved in Meso-NH research, along with the international ACCORD. For the present study, the authors acknowledge Denis Brion (Meteo-France) for providing the gridded daily temperature data for the Ile-de-France region, SIRTA and FLUXNET Network for providing the radiation station data, Isabelle Pfaffenzeller (Meteo-France) for providing the COMEPHORE dataset (available through AERIS platform : https://radarsmf.aeris-data.fr/), and Robin Lagarrigue (Santé Publique France) for providing heat-wave warning threshold data. The authors would also thank Samuel Somot for his comments and advice for some climatic analyses. consortium. This work was partly supported by the French National Agency under the future investment program ANR-18-MPGA-0005.

References

Bokwa A, Hajto MJ, Walawender JP, Szymanowski M (2015). Influence of diversified relief on the urban heat island in the city of Kraków, Poland. Theor Appl Climatol 122:365–382. https://doi.org/10.1007/s00704-015-1577-9

Boone A, Masson V, Meyers T, Noilhan J (2000) The influence of the inclusion of soil freezing on simulations by a soil–vegetation–atmosphere transfer scheme. J Appl Meteor 39:1544-1569. https://doi.org/10.1175/1520-0450(2000)039<1544:TIOTIO>2.0.CO;2

Boone A, Calvet J-C, Noilhan J (1999) The inclusion of a third soil layer in a Land Surface Scheme using the Force-Restore method. J Appl Meteor 38:1611–1630. https://doi.org/10.1175/1520-0450(1999)038<1611:IOATSL>2.0.CO;2

Brousseau P, Seity Y, Ricard D, Léger J (2016) Improvement of the forecast of convective activity from the AROME-France system. Q J R Meteorol Soc 142:2231–2243. https://doi.org/10.1002/qj.2822

Caillaud C, Somot S, Alias A, Bernard-Bouissières I, Fumière Q, Laurantin O, Seity Y, Ducrocq V (2021) Modelling Mediterranean heavy precipitation events at climate scale: an object-oriented evaluation of the CNRM-AROME convection-permitting regional climate model. Clim Dyn 56:1717–1752. https://doi.org/10.1007/s00382-020-05558-y

Carabajal CC, Harding DJ, Boy J-P, Danielson JJ, Gesch DB, Suchdeo VP (2011) Evaluation of the Global Multi-Resolution Terrain Elevation Data 2010 (GMTED2010) using ICESat geodetic control, Proc. SPIE 8286, International Symposium on Lidar and Radar Mapping 2011: Technologies and Applications, 82861Y.

Champeaux J-L, Masson V, Chauvin F (2005) ECOCLIMAP: a global database of land surface parameters at 1 km resolution. Met Apps 12:29–32. https://doi.org/10.1017/S1350482705001519

Coppola E, Sobolowski S, Pichelli E, Raffaele F, Ahrens B, Anders I, Ban N, Bastin S, Belda M, Belusic D, A. Caldas-Alvarez A, Cardoso RM, Davolio S, Dobler A, Fernandez J, Fita L, Fumiere Q, Giorgi F, Goergen, K, Güttler I, Halenka T, Heinzeller D, Hodnebrog Ø, Jacob D, Kartsios S, Katragkou E, Kendon E, Khodayar S, Kunstmann H, Knist S, Lavín-Gullón A, Lind P, Lorenz T, Maraun D, Marelle L, van Meijgaard E, Milovac J, Myhre G,.Panitz H-J, Piazza M, Raffa M, Raub T, Rockel B, Schär C, Sieck K, M. Soares PM, Somot S, Srnec L, Stocchi P, Tölle MH, Truhetz H, Vautard R, de Vries H, Warrach-Sagi K (2020). A first-of-its-kind multi-model convection permitting ensemble for investigating convective phenomena over Europe and the Mediterranean. Clim Dyn 55(1):3–34. https://doi.org/10.1007/s00382-018-4521-8

Daniel M, Lemonsu A, Déqué M, Somot S, Alias A, Masson V (2019). Benefits of explicit urban parameterization in regional climate modeling to study climate and city interactions. Clim Dyn 52(5–6):2745–2764. https://doi.org/10.1007/s00382-018-4289-x

Decharme B, Boone A, Delire C, Noilhan J (2011) Local evaluation of the Interaction between Soil Biosphere Atmosphere soil multilayer diffusion scheme using four pedotransfer functions. J Geophys Res 116:D20126. https://doi.org/10.1029/2011JD016002

Dee DP, Uppala S, Simmons A, Berrisford P, Poli P, Kobayashi S, Andrae U, Balmaseda M, Balsamo G, Bauer dP, Bechtold P, Beljaars ACM, van de Berg L, Bidlot J, BormannN, Delsol C, Dragani R, Fuentes M, Geer AJ, Haimberger L, Healy SB, Hersbach H, Hólm EV, Isaksen L, Kållberg P, Köhler M, Matricardi M, McNally AP, Monge-Sanz BM, Morcrette J-J, Park B-K, Peubey C, de Rosnay P, Tavolato C, Thépaut J-N, Vitart F (2011) The ERA-Interim reanalysis: configuration and performance of the data assimilation system. Q J R Meteorol Soc 137(656):553–597. https://doi.org/10.1002/qj.828

Déqué M, Alias A, Somot S, Nuissier O (2016) Climate change and extreme precipitation: the response by a convection-resolving model. In: Research activities in atmospheric and oceanic modelling CAS/JSC Working group on numerical experimentation Report No. 46

Faroux F, Kaptué Tchuenté AT, Roujean J-L, Martin E, Masson V, Le Moigne P (2013) ECOCLIMAP-II/Europe : a twofold database of ecosystems and surface parameters at 1-km resolution based on satellite information for use in land surface, meteorological and climate models. Geosci Model Dev 6:563–582. https://doi.org/10.5194/gmd-6-563-2013

Founda D, Santamouris M (2017) Synergies between Urban Heat Island and Heat Waves in Athens (Greece), during an extremely hot summer (2012). Sci Rep 7:10973. https://doi.org/10.1038/s41598-017-11407-6

Fumière Q, Déqué M, Nuissier O, Somot S, Alias A, Caillaud C, Laurantin O, Seity Y (2020) Extreme rainfall in Mediterranean France during the fall: added value of the CNRM-AROME convection-permitting regional climate model. Clim Dyn 55:77–91. https://doi.org/10.1007/s00382-019-04898-8

Haeffelin M, Barthès L, Bock O, Boitel C, Bony S, Bouniol D, Chepfer H, Chiriaco M, Cuesta J, Delanoë J, Drobinski P, Dufresne J-L, Flamant C, Grall M, Hodzic A, Hourdin F, Lapouge F, Lemaître Y, Mathieu A, Morille Y, Naud C, Noël V, O'Hirok W, Pelon J, Pietras C, Protat A, Romand B, Scialom G, Vautard R (2005) SIRTA, a ground-based atmospheric observatory for cloud and aerosol research. Ann Geophys 23:253–275. https://doi.org/10.5194/angeo-23-253-2005

Hamdi R, Masson V (2008) Inclusion of a drag approach in the town energy balance (TEB) scheme : offline 1-d validation in a street canyon. J Appl Meteor Climatol 47:2627–2644. https://doi.org/10.1175/2008JAMC1865.1

He B-J (2018) Potentials of meteorological characteristics and synoptic conditions to mitigate urban heat island effects. Urban Climate 24:26-33. https://doi.org/10.1016/j.uclim.2018.01.004

Hewitt CD, Lowe JA (2018). Toward a European climate prediction system. Bull Am Meteorol Soc 99(10):1997–2001. https://doi.org/10.1175/BAMS-D-18-0022.1

IPCC (2022) Climate Change 2022: Impacts, Adaptation, and Vulnerability. Contribution of Working Group II to the Sixth Assessment Report of the Intergovernmental Panel on Climate Change [Pörtner H-O, Roberts DC, Tignor M, Poloczanska ES, Mintenbeck K, Alegría A, Craig M, Langsdorf S, Löschke S, Möller V, Okem A, Rama B (eds.)]. Cambridge University Press. In Press

Jacob D, Petersen J, Eggert B Alias A, Bøssing Christensen O, Bouwer LM, Braun A, Colette A, Déqué M, Georgievski G, Georgopoulou E, Gobiet A, Menut L, Nikulin G, Haensler A, Hempelmann N, Jones C, Keuler K, Kovats S, Kröner N, Kotlarski S, Kriegsmann A, Martin E, van Meijgaard E, Moseley C, Pfeifer S, Preuschmann S, Radermacher C, Radtke K, Rechid D, Rounsevell M, Samuelsson P, Somot S, Soussana J-F, Teichmann C, Valentini R, Vautard R, Weber B, Yiou P (2014) EURO-CORDEX: new high-resolution climate change projections for European impact research. Reg Environ Change 14:563–578. https://doi.org/10.1007

Kassomenos P, Kissas G, Petrou I, Begou P, Khan HS, Santamouris M (2022) The influence of daily weather types on the development and intensity of the urban heat island in two Mediterranean coastal metropolises. Sci Total Env 819:153071. https://doi.org/10.1016/j.scitotenv.2022.153071

Kounkoud-Arnaud R, Brion D (2018) Optimal interpolation of daily temperatures around Paris, taking into account urban fraction. 10th International Conference on Urban Climate. New York, NY: Am Meteor Soc. https://ams.confex.com/ams/ICUC10/meetingapp.cgi/Paper/341760

Le Roy B, Lemonsu A, Kounkou-Arnaud R, Brion D, Masson V (2020) Long time series spatialized data for urban climatological studies: a case study of Paris, France. Int J Climatol 40(7):3567–3584. https://doi.org/10.1002/joc.6414

Lemonsu A, Masson V, Shashua-Bar L, Erell E, Pearlmutter D (2012) Inclusion of vegetation in the Town Energy Balance model for modelling urban green areas. Geosci Model Dev 5:1377–1393. https://doi.org/10.5194/gmd-5-1377-2012

Laaidi K, Zeghnoun A, Dousset B, Bretin P, Vandentorren S, Giraudet E, Beaudeau P (2012) The impact of heat islands on mortality in Paris during the August 2003 heat wave. Environ Health Perspectives 120(2):254–9. https://ehp.niehs.nih.gov/doi/10.1289/ehp.1103532

Liu J, Niyogi D (2019) Meta-analysis of urbanization impact on rainfall modification. Sci Rep 9:7301. https://doi.org/10.1038/s41598-019-42494-2

Lorenz JM, Kronenberg R, Bernhofer C, Niyogi D (2019). Urban rainfall modification: Observational climatology over Berlin, Germany. Journal of Geophysical Research: Atmospheres 124:731–746. https://doi.org/10.1029/2018JD028858

Lucas-Picher P, Brisson E, Caillaud C, Alias A, Nabat P, Lemonsu A, Poncet N, Cortes Hernandez VE, Michau Y, Doury A, Monteiro D, Somot S (2022) Evaluation of the convection-permitting regional climate model CNRM-AROME41t1 over northwestern Europe. Clim Dyn. Submitted.

Lucas-Picher P, Argüeso D, Brisson E, Tramblay Y, Berg P, Lemonsu A, Kotlarski S, Caillaud C (2021) Convection-permitting modeling with regional climate models: Latest developments and next steps. Wiley Interdisciplinary Reviews: Climate Change 12(6):e731. https://doi.org/10.1002/wcc.731

Masson V, Lemonsu A, Hidalgo J, Voogt J (2020) Urban Climates and Climate Change. Annual Review of Environment and Resources 45:411–444. https://doi.org/10.1146/annurev-environ-012320-083623

Masson V, Le Moigne P, Martin E, Faroux S, Alias A, Alkama R, Belamari S, Barbu A, Boone A, Bouyssel F, Brousseau P, Brun E, Calvet J-C, Carrer D, Decharme B, Delire C, Donier S, Essaouini K, Gibelin A-L, Giordani H, Habets F, Jidane M, Kerdraon G, Kourzeneva E, Lafaysse M, Lafont S, Lebeaupin Brossier C, Lemonsu A, Mahfouf J-F, Marguinaud P, Mokhtari M, Morin S, Pigeon G, Salgado R, Seity Y, Taillefer F, Tanguy G, Tulet P, Vincendon B, Vionnet V, Voldoire A (2013) The SURFEXv7.2 land and ocean surface platform for coupled or offline simulation of Earth surface variables and fluxes. Geosci Model Dev 6:929–960. https://doi.org/10.5194/gmd-6-929-2013

Masson V, Seity Y (2009) Including atmospheric layers in vegetation and urban offline surface schemes. Journal of Applied Meteorology and Climatology 48(7):1377–1397. https://doi.org/10.1175/2009JAMC1866.1

Masson V, Champeaux J-L, Chauvin F, Meriguet C, Lacaze R (2003) A global data base of land surface parameters at 1 km resolution in meteorological and climate models. J of Climate 16:1261–1282. https://doi.org/10.1175/1520-0442(2003)16<1261:AGDOLS>2.0.CO;2

Masson V (2000) A Physically-based scheme for the Urban Energy Budget in atmospheric models. Boundary-Layer Meteorol. 94:357–397. https://doi.org/10.1023/A:1002463829265

Melecio-Vázquez D, Ramamurthy P, Arend M, González-Cruz JE (2018) Thermal Structure of a Coastal–Urban Boundary Layer. Boundary-Layer Meteorol 169:151–161. https://doi.org/10.1007/s10546-018-0361-7

Michau Y, Lemonsu A, Lucas-Picher P, Caillaud C, Alias A (2022) Urban climate assessment using the CNRM-AROME CPM: the case of 12 French cities. Clim Dyn. Submitted.

Nabat P, Somot S, Cassou C, Mallet M, Michou M, Bouniol D, Decharme B, Drugé T, Roehrig R, Saint-Martin D (2020) Modulation of radiative aerosols effects by atmospheric circulation over the Euro-Mediterranean region. Atmospheric Chemistry and Physics 20(14):8315–8349. https://doi.org/10.5194/acp-20-8315-2020

Nachtergaele F, Velthuizen H, Verelst L, Wiberg D (2012) Harmonized World Soil Database Version 1.2, FAO/IIASA/ISRIC/ISS-CAS/JRC.

Ngarambe J, Oh JW, Su MA, Santamouris M, Yun GY (2021) Influences of wind speed, sky conditions, land use and land cover characteristics on the magnitude of the urban heat island in Seoul: An exploratory analysis. Sustainable Cities and Society 71:102953. https://doi.org/10.1016/j.scs.2021.102953

Noilhan J, Planton S (1989) A simple parameterization of land surface processes for meteorological models. Mon Weather Rev 117(3):536–549. https://doi.org/10.1175/1520-0493(1989)117<0536:ASPOLS>2.0.CO;2

Oke T, Mills G, Christen A, Voogt J (2017). Urban Climates. Cambridge: Cambridge University Press. https://doi.org/10.1017/9781139016476

Pascal M, Lagarrigue R, Tabai A, Bonmarin I, Camail S, Laaidi K, Le Tertre A, Denys S (2021) Evolving heat waves characteristics challenge heat warning systems and prevention plans. Int J Biometeorol 65:1683–1694. https://doi.org/10.1007/s00484-021-02123-y

Pergaud J, Masson V, Malardel S, Couvreux F (2009) A Parameterization of Dry Thermals and Shallow Cumuli for Mesoscale Numerical Weather Prediction. Boundary-Layer Meteorol 132:83–106. https://doi.org/10.1007/s10546-009-9388-0

Philip A, Bergot T, Bouteloup Y, Bouyssel F (2016) The impact of vertical resolution on fog forecasting in the kilometric-scale model arome: a case study and statistics. Weather and Forecasting 31:1655–1671. https://doi.org/10.1175/WAF-D-16-0074.1

Pigeon G, Zibouche K, Bueno B, Le Bras J, Masson V (2014) Improving the capabilities of the Town Energy Balance model with up-to-date building energy simulation algorithms: an application to a set of representative buildings in Paris. Energy and Buildings 76:1–14. https://doi.org/10.1016/j.enbuild.2013.10.038

Prein AF, Langhans W, Fosser G, Ferrone A, Ban N, Goergen K, Keller M, Tölle M, Gutjahr O, Feser F, Brisson E, Kollet S, Schmidli J, van Lipzig NPM, Leung R (2015) A review on regional convection-permitting climate modeling: Demonstrations, prospects, and challenges. Reviews of geophysics 53(2):323–361. https://doi.org/10.1002/2014RG000475

Santamouris M, Haddad S, Fiorito F, Osmond P, Ding L, Prasad D, Zhai X, Wang R (2017) Urban Heat Island and Overheating Characteristics in Sydney, Australia. An Analysis of Multiyear Measurements. Sustainability, 9:712. https://doi.org/10.3390/su9050712

Schinasi LH, Benmarhnia T, De Roos AJ (2018) Modification of the association between high ambient temperature and health by urban microclimate indicators: A systematic review and meta-analysis. Environmental research 161:168–80. https://doi.org/10.1016/j.envres.2017.11.004

Seity Y, Brousseau P, Malardel S, Hello G, Bénard P, Bouttier F, Lac C, Masson V (2011) The AROME-France convective-scale operational model. Monthly Weather Review 139(3):976–991. https://doi.org/10.1175/2010MWR3425.1

Tabary P, Dupuy P, Lhenaff G, Gueguen C, Moulin L, Laurantin O, Merlier C, Soubeyroux JM (2012) A 10-year (1997-2006) reanalysis of Quantitative Precipitation Estimation over France: methodology and first results. In: IAHS-AISH publication, pp 255–260

Tan J, Zheng Y, Tang X, Guo C, Li L, Song G, Zhen X, Yuan D, Kalkstein AJ, Li F, Chen H. (2010) The urban heat island and its impact on heat waves and human health in Shanghai. Int J Biometeorol 54:75–84. pmid:19727842. https://doi.org/10.1007/s00484-009-0256-x

Termonia P, Fischer C, Bazile E, Bouyssel F, Brožková R, Bénard P, Bochenek B, Degrauwe D, Derková M, El Khatib R et al (2018) The ALADIN system and its canonical model configurations AROME CY41T1 and ALARO CY40T1. Geosci Model Dev 11(1):257. https://doi.org/10.5194/gmd-11-257-2018

Theeuwes NE, Barlow JF, Teuling AJ, Grimmond CSB, Kotthaus S (2019) Persistent cloud cover over mega-cities linked to surface heat release. npj Climate and Atmospheric Science 2:15. https://doi.org/10.1038/s41612-019-0072-x

Tong S, Wong NH, Tan CL, Jusuf SK, Ignatius M, Tan E (2017) Impact of urban morphology on microclimate and thermal comfort in northern China. Solar Energy 155:212–223. https://doi.org/10.1016/j.solener.2017.06.027

Tsiringakis A, Theeuwes NE, Barlow JF, Steeneveld G-J (2022). Interactions Between the Nocturnal Low-Level Jets and the Urban Boundary Layer: A Case Study over London. Boundary-Layer Meteorol 183:249–272. https://doi.org/10.1007/s10546-021-00681-7

Wang M, Tang G, Liu Y, Ma M, Yu M, Hu B, Zhang Y, Wang Y, Wang Y (2021) The difference in the boundary layer height between urban and suburban areas in Beijing and its implications for air pollution. Atmospheric Environment 260:118552. https://doi.org/10.1016/j.atmosenv.2021.118552

Yang J, Hu L, Wang C. Population dynamics modify urban residents' exposure to extreme temperatures across the United States. Sci Adv 5(12):eaay3452. https://doi.org/10.1126/sciadv.aay3452

Zhang Y, Zhang J, Zhang X, Zhou D, Gu Z (2021) Analyzing the Characteristics of UHI (Urban Heat Island) in Summer Daytime Based on Observations on 50 Sites in 11 LCZ (Local Climate Zone) Types in Xi'an, China. Sustainability, 13:83 https://doi.org/10.3390/su13010083